To appear in: Topology-Based Methods in Mathematics + Visualization, Springer 2007

Visualizing Lagrangian Coherent Structures and Comparison to Vector Field Topology

Filip Sadlo and Ronald Peikert

Computer Graphics Laboratory, Computer Science Department,
ETH Zurich, Switzerland {sadlo, peikert}@inf.ethz.ch

This paper takes a look at the visualization side of vector field analysis based on Lagrangian coherent structures. The Lagrangian coherent structures are extracted as height ridges of finite-time Lyapunov exponent fields. The resulting visualizations are compared to those from traditional instantaneous vector field topology of steady and unsteady vector fields: they often provide more and better interpretable information. The examination is applied to 3D vector fields from a dynamical system and practical CFD simulations.

1 Introduction

Vector field topology (VFT) is often used to obtain a simplified representation of a vector field or phase space of a dynamical system. Introduced to the visualization community by Helman et al. [HH89], it also allows deeper insight into the structure of vector fields. VFT deals with the detection, classification and global analysis of critical points (isolated zeros of the vector field). The manifolds that are defined by the eigenvectors of the velocity gradient at these points can be computed by integrating streamlines (for 1D manifolds) or stream surfaces (for 2D manifolds). According to the eigenvalues, the manifolds can be stable (negative real part) or unstable (positive real part). In other words, a stable manifold is the set of all trajectories that converge to the critical point in positive time [Asi93]. The manifolds are also called separatrices because they separate regions of different flow behavior in the respective direction of time.

However, there is one important drawback of the method: it is meaningful in a direct sense only for steady vector fields (autonomous dynamical systems). One reason for this limitation is that pathlines usually diverge from streamlines and that critical points often move in unsteady vector fields. Unsteady vector fields are often analyzed by VFT of isolated time steps. Although this is hard to interpret and gives no precise information about the true behavior, it gives an instantaneous picture and can give insight especially when applied

To appear in: Topology-Based Methods in Mathematics + Visualization, Springer 2007

to derived fields. Other approaches to a time-dependent topology based on path lines are that of Theisel et al. [TWH*04] and Shi et al. [STW*06].

The advantage of the concept of coherent structures (Section 2) is that it shows the true behavior, is clearly physically motivated, scale-aware and therefore noise-insensitive, and easy interpretable, even for unsteady vector fields.

This paper describes the concept of Lagrangian coherent structures and how they are obtained by filtered ridge extraction from finite-time Lyapunov exponent in Section 2. In Section 3 FTLE ridges are extracted from steady and unsteady 3D vector field examples and compared to vector field topology.

2 Lagrangian Coherent Structures

In recent years, the concept of Lagrangian coherent structures (LCS) is attracting attention in the field of vector field analysis, especially since Haller [Hal01] has shown that LCS can be obtained by detecting local extrema in the finite-time Lyapunov exponent (FTLE) (explained in Section 2.1). Material lines or surfaces (LCS) are attracting if infinitesimal perturbations converge to these structures in forward time and repelling if they are attracting in backward time. According to Haller [Hal01], attracting LCS can be obtained as local maxima, or ridges (approximated as height ridges described in Section 2.2), of backward-time FTLE, and the repelling ones as ridges in forward-time FTLE. Stable and unstable manifolds tend to have its analog in repelling and attracting material lines or surfaces, at least for steady vector fields (see also results in Section 3). In contrast to vector field topology, LCS tend to be insensitive to short-term perturbations and small-scale noise, such as turbulence, due to their Lagrangian definition. Additionally, LCS are usually more appropriate for unsteady vector fields due to their clear physical motivation and interpretability. Note that LCS of unsteady fields usually deform and move over time but are still easy to interpret.

2.1 Finite-Time Lyapunov Exponent

The finite-time Lyapunov exponent (FTLE) measures the separation (or expansion) rate of nearby particles when advected by the flow for a given time T. For a n-dimensional vector field, there are n Lyapunov exponents. Here we are only interested in the largest FTLE. It is a scalar Lagrangian measure stored at the starting point of the respective trajectory. According to Haller [Hal01] the FTLE can be computed by advecting each sample point $\mathbf{x} \in D$ of an arbitrary grid at time t_0 with the flow for time T, resulting in a flow map $\boldsymbol{\phi}_{t_0}^{t_0+T}(\mathbf{x})$ that maps $\mathbf{x}$ to its advected position. We decided to stop the advection if the point reaches a domain boundary and store the position on the boundary in the flow map.

To appear in: Topology-Based Methods in Mathematics + Visualization, Springer 2007

The maximum separation of two close particles can be computed from the gradient of the flow map: it is the spectral norm of its gradient. In other words: to measure the maximum separation one has to seed the two particles along the direction of maximum expansion, which is the direction of the eigenvector belonging to the largest eigenvalue of

$$\Delta(\mathbf{x}) = (\nabla \boldsymbol{\phi}_{t_0}^{t_0+T}(\mathbf{x}))^\top \cdot \nabla \boldsymbol{\phi}_{t_0}^{t_0+T}(\mathbf{x}). \tag{1}$$

(1) is called the Right Cauchy-Green deformation tensor, measuring the square of the distance change due to deformation. Accordingly, the maximum separation is the square root of the largest eigenvalue of $\Delta(\mathbf{x})$. Lyapunov exponents are used to measure exponential growth rates of perturbations. Therefore the logarithm of the resulting value is computed and additionally normalized by absolute advection time $|T|$, leading to the following formulation for the largest FTLE denoted as $\sigma_{t_0}^T$:

$$\sigma_{t_0}^T(\mathbf{x}) = \frac{1}{|T|} ln \sqrt{\lambda_{max}(\Delta(\mathbf{x}))}. \tag{2}$$

The reader is referred to the work of Haller for further information on LCS and FTLE [Hal01, Hal02], and vortices and FTLE [Hal05].

2.2 Height Ridges

Height ridges are local maxima in a relaxed sense. More precisely, height ridges are locations where a scalar field s has a local maximum in at least one direction. More general, height ridges are d-dimensional manifolds in n-dimensional space with $n > d \geq 0$.

The ridge criterion can be formulated using the gradient and the Hessian of s. Note that for a height ridge, the eigenvectors belonging to the d largest eigenvalues λ_i $(i = 1, \ldots, d)$ of the Hessian point along the ridge, whereas the eigenvectors of the $(n - d)$ smallest eigenvalues λ_j $(j = d + 1, \ldots, n)$ point orthogonally to the ridge. One necessary condition for a ridge is that the derivatives in λ_j-eigenvector directions are zero. This leads to the condition

$$\boldsymbol{\epsilon}_{\lambda_j} \cdot \nabla s = 0 \tag{3}$$

with $\boldsymbol{\epsilon}_{\lambda_j}$ the eigenvector belonging to λ_j. The other condition for a height ridge is that the second derivatives in $\boldsymbol{\epsilon}_{\lambda_j}$ directions are negative, formulated as

$$\lambda_j < 0. \tag{4}$$

Valley lines (the opposite of height ridges) are obtained by computing height ridges of the field $-s$. The reader is referred to the work of Eberly [Ebe96], Lindeberg [Lin96], and the thesis of Majer [Maj00] for further details.

For the extraction of 2D ridges in the 3D domain, one would like to use e.g. *Marching Cubes*. However, since an eigenvector is not oriented, direct application of these methods to (3) fails because the eigenvectors at the nodes

To appear in: Topology-Based Methods in Mathematics + Visualization, Springer 2007

of a cell can be inconsistently oriented. For their *Marching Ridges*, Furst et al. [FP01] use PCA to achieve local consistency of the eigenvectors of a cell. Kindlmann et al. [KTW06] achieve per-cell eigenvector consistency by sampling along each edge of the cell and observing eigenvector rotation. Inter-cell consistency is circumvented by a subsequent pass over the triangles that fixes their orientation.

In this work, per-cell eigenvector consistency is guided by PCA of the eigenvectors at the nodes of the cell, according to Furst et al.. We experienced non-orientable ridge surfaces in some applications. Flat shading and bi-directional lighting was chosen in these cases.

2.3 FTLE Ridge Filtering

Because ridge extraction involves computation of second derivatives, noise amplification can become an issue. Smoothing is applied in these cases in order to obtain significant visualizations. One has to keep in mind however, that this tends to deform the LCS, i.e. particles can permeate the computed FTLE ridges to a certain degree. It is therefore advisable to verify the LCS using trajectories (for steady vector fields) or animations of LCS and particles (unsteady vector fields).

Smoothing is realized by incorporating it into the gradient computation. In our case, the gradient at a given node is computed by fitting a linear vector field to its neighboring nodes in a Least Squares sense. The degree of smoothing can be controlled by adjustment of the neighborhood range.

The finite-time Lyapunov exponent measures the amount of separation. It is therefore straight-forward to use it to filter out parts of ridges with low separation property. This approach is physically motivated and therefore results in relevant and consistent visualizations. It is therefore our favorite method for FTLE ridge filtering.

Filtering connected components of the final mesh by their area is also an effective method for improving the visualization. Small connected components of ridges are likely to be noise, as long as the other filtering conditions did not disrupt the ridges because of low tolerance.

Another approach is to use the second derivative across the ridge (λ_n) for filtering out "flat" ridges. Although it turned out that its effect was comparable to filtering by FTLE in our examples, it is only geometrically motivated and therefore less preferable. Therefore it was not used for the results in Section 3, except for the vortex ring in Section 3.4.

In order to filter out ridges that arise due to trajectories that reach the domain boundary, it is allowed to filter out ridge regions by advection time of the corresponding trajectories. As noted in Section 2.1, pathline integration is stopped if the particle reaches a domain boundary. The advection time is smaller than T in these cases and a threshold can be used for suppressing them.

To appear in: Topology-Based Methods in Mathematics + Visualization, Springer 2007

During ridge extraction by marching ridges (Section 2.2), the necessary ridge condition (4) and filtering conditions are tested at the vertices of the resulting triangles and triangles that violate them are rejected. Triangle trimming was not implemented in the current approach, leading to zigzag ridge borders. Figures 9(c)–9(e) show an example of FTLE ridge filtering.

3 Results

The described methods are applied to different vector fields. The first example is the analytic and steady ABC flow (Section 3.1). Then 3D saddles in isolated time steps of an unsteady Francis water turbine CFD simulation are examined (Section 3.2), and vector field topology is compared to FTLE ridges. In Section 3.3 the flow around the divider of the same CFD result is analyzed but this time both, in a steady and unsteady manner. Section 3.4 takes again a look at the Francis dataset, but this time at two vortices. Finally, Section 3.5 examines a steady-type Pelton water turbine CFD simulation.

3.1 ABC Flow

Vector field topology and FTLE ridges are applied to the analytic steady ABC flow field. This flow has three parameters A, B, and C, (in this example set to $\sqrt{3}$, $\sqrt{2}$, and 1 according to Henon [Hen66]) named after the researchers Arnold, Beltrami, and Childress, and can be written as the dynamical system

$$\begin{aligned} \dot{x} &= A \sin z + C \cos y \\ \dot{y} &= B \sin x + A \cos z \,. \\ \dot{z} &= C \sin y + B \cos x \end{aligned} \tag{5}$$

It is triple-periodic in space and divergence-free. Despite of its simple Eulerian nature, it exhibits complicated Lagrangian structure such as invariant tori and chaotic advection [HZD98] if considered as a three-dimensional torus. Other interesting properties are that it is identical to its curl and therefore fully helical. This is the cause why vortex core line detection based on helicity, such as that by Levy et al. [LDS90], fail on this flow. The ABC field was discretized on a regular grid in order to show the applicability of the method to practical vector fields.

Figure 8(a) shows the VFT view to the field. Critical points have been determined and streamlines have been computed in positive and negative time. Streamlines are seeded on two rings of seeds around the critical point. The circles are usually chosen coplanar with the 2D manifold, have user defined radius and user defined offset along the direction of the 1D manifold. Unfortunately it turns out that the 2D manifolds are degenerate in this case of the ABC flow, meaning that one eigenvalue of the velocity gradient is zero. Therefore this is a steady case where the vector field topology approach fails or may not be practical to give a complete image of the flow structure.

To appear in: Topology-Based Methods in Mathematics + Visualization, Springer 2007

Haller already investigated the ABC flow using FTLE [Hal01], but without extracting ridges. Figures 8(b)–8(d) show the LCS view to the field using ridges. It can be seen that the ridges are consistent with the manifolds: the critical points are located at the intersection of positive-time and negative-time FTLE ridges, and the streamlines in positive and negative time follow the corresponding ridges. FTLE was only computed at the "original" nodes in the first period of the ABC flow consisting of 30^3 nodes, but the integration time of 2 caused the trajectories to reach neighboring periods of the ABC flow as well. Ridges were only generated in regions with FTLE higher or equal to 0.9 for suppressing weak separation phenomena, gradient neighborhood range for smoothing during ridge extraction was 2 (as in all examples), and connected components below 50 triangles have been suppressed. The computation took 113 seconds. Figures 9(a) and 9(b) show another view and some of the trajectories used for computation.

To also visualize the short-time separation aspect of the flow, short-time FTLE was computed and color-coded on the long-time FTLE ridges. Figure 8(e) shows the result of integration time +0.001 (which took 22 seconds) on the positive-time ridges. It can be seen that the short-time FTLE exhibits local maxima near the critical points. Figure 8(f) shows additionally the negative-time ridges with short-time FTLE of integration time -0.001. There are also local maxima of the FTLE near the critical points in negative time direction. From the streamlines it can be seen, that the local maxima are not in upstream or downstream direction of the critical points, as one may assume. It has to be investigated to what extent this situation is sensitive to noise and if it is a specialty of the ABC flow or a general principle.

3.2 3D Saddles in Francis Draft Tube

In this section the LCS and VFT approaches are compared for non-spiralling 3D saddles. As a first step one would think of applying the methods to an analytic linear vector field containing a saddle, described by a Jacobian with real eigenvalues. VFT performs well in these cases, unless the 2D manifold of the saddle is degenerate as in Section 3.1. However, the FTLE ridge approach is not able to capture linear saddles because all trajectories through it would exhibit the same FTLE value and therefore there would be no ridges corresponding to its manifolds. This is a drawback of the FTLE ridge approach.

However, it is unlikely that purely linear saddle regions appear in practical vector fields. Therefore the examination was applied to some of the saddles in a CFD simulation of the draft tube of a Francis water turbine. As a first approach, a single time step of the unsteady simulation was used for the analysis. This results in instantaneous LCS based on streamlines, suited for the comparison of VFT and LCS methods. The critical points were detected and at each critical point two FTLE were computed on a regular grid of 60^3 nodes around the critical point, one with integration time $+1$ second and one with -1 second. Computation at the first saddle took 321 and 427 seconds,

To appear in: Topology-Based Methods in Mathematics + Visualization, Springer 2007

respectively. Confer 9(d) and 9(e) for filtering details. The extracted ridges are shown in Figures 9(f), 9(g), and 1. Figure 4 shows some streamlines used for FTLE computation of Figure 1.

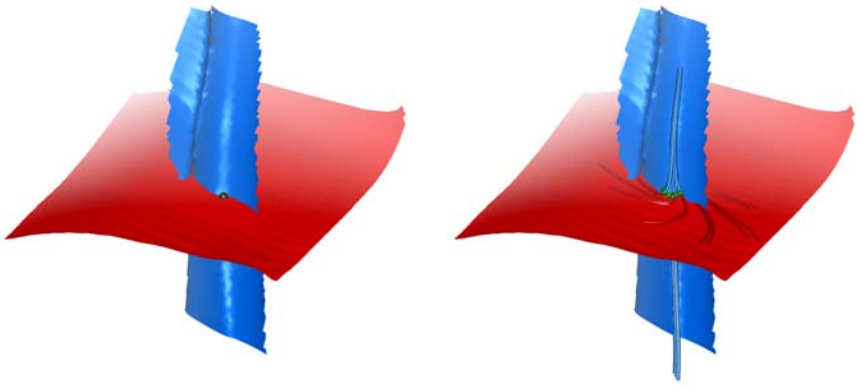

Fig. 1. Another 3D saddle in Francis draft tube. Same visualization as in Figures 9(f) and 9(g).

One can see that the 2D manifolds are well captured by the corresponding ridges, resulting in smooth surfaces. It has to be noted that also the opposite-time FTLE ridges result in surfaces, even though these surfaces exhibit more curvature and folding. It can be seen that these ridges are well consistent with the 1D manifolds of the saddles. We conclude that: the examined critical points lie on the intersection curves of positive-time and negative-time FTLE ridges. This was also observed in the ABC flow example of Section 3.1. The 2D manifolds have a ridge counterpart and the 1D manifolds are consistent with the corresponding opposite-time 2D ridge. Therefore, generating FTLE ridges in positive and negative time in regions around critical points tends to convey more information than traditional VFT and can serve as topological icons. Extracting and visualizing the intersection curves of positive-time and negative-time FTLE ridges, similar to the saddle connectors of Theisel et al. [TWH*03], seems promising and could serve as a kind of a topological skeleton, which could be applicable even for unsteady vector fields.

Although our investigation did not result in any "purely linear" 3D saddle regions in CFD simulations, it has to be examined how frequent they are in practical vector fields and what extent they have. The extent is of some importance because the FTLE ridge approach fails if the trajectories do not escape from the linear regime of the vector field. Another thing to note is that for short advection times $|T|$ the FTLE ridges tend to be less smooth, smaller, and less consistent with VFT. This turned out to be a problem for getting the unsteady positive and negative time FTLE ridges on the saddles:

To appear in: Topology-Based Methods in Mathematics + Visualization, Springer 2007

the temporal domain of the simulation was too short with respect to the low velocities in the region where the saddles reside.

3.3 Bifurcation in Francis Draft Tube

In this section the unsteady CFD flow around the divider of the Francis draft tube is analyzed using steady and unsteady FTLE ridges. The divider is a construct that divides the flow into the two channels. First, instantaneous FTLE ridges were computed at the first time step of the simulation. Figure 2 (left) shows some of the positive-time streamlines used for FTLE computation, Figure 2 (right) shows additionally the resulting ridge. One can see that the ridge is deformed at the horizontal vortex core line (computed according to Levy et al. as in all examples) in the upper part of the image. However, the ridge does not exhibit a hole where it intersects that vortex core line. For the instantaneous flow, this can be interpreted that the flow passes the vortex core line at a critical point and is finally separated at the divider. On the other hand, the ridge forms a tunnel around the vortex core line at the bottom of the image. This is a case where the vortex is captured as a distinct LCS.

Next, the instantaneous FTLE ridge of the first time step is compared to the unsteady FTLE ridge of the first time step. Figure 3 shows the corresponding visualizations. Both steady and unsteady FTLE ridges were computed on a $30 \times 40 \times 50$ grid using an advection time of 0.4 seconds and filtered by requiring a minimum FTLE of 7.1. The computation took 631 seconds in the steady case and 1255 seconds in the unsteady case. In order to remove other ridges that were not consistent with the ridge under consideration, the minimal connected component size was set to 2000 triangles. It is clearly visible that the unsteady FTLE ridge differs in shape from the steady FTLE ridge. One difference is that it does not divide the flow on the left hand side anymore. Instead, it extends only to the right. Some trajectories are crossing the unsteady ridge. This is likely to happen for unsteady LCS because they are material surfaces at a given time whereas trajectories extend over time and are immaterial. Trajectories with nearby seeds are visualizing the mechanisms of separation.

3.4 Vortices in Francis Draft Tube

Vortices are coherent structures and therefore they should show up in FTLE ridge visualizations. Two vortices are examined, both using instantaneous FTLE ridges because of the small temporal domain of the underlying CFD simulation. The first vortex is in front of the divider from Section 3.3, but this time at the last time step. Figure 5 shows the positive-time FTLE ridges of this vortex. The vortex is nicely captured by the FTLE ridge that is also indicating the separation by the divider. The grid consisted of $30 \times 40 \times 50$ nodes, advection time was 0.4 seconds, ridge regions with FTLE smaller

To appear in: Topology-Based Methods in Mathematics + Visualization, Springer 2007

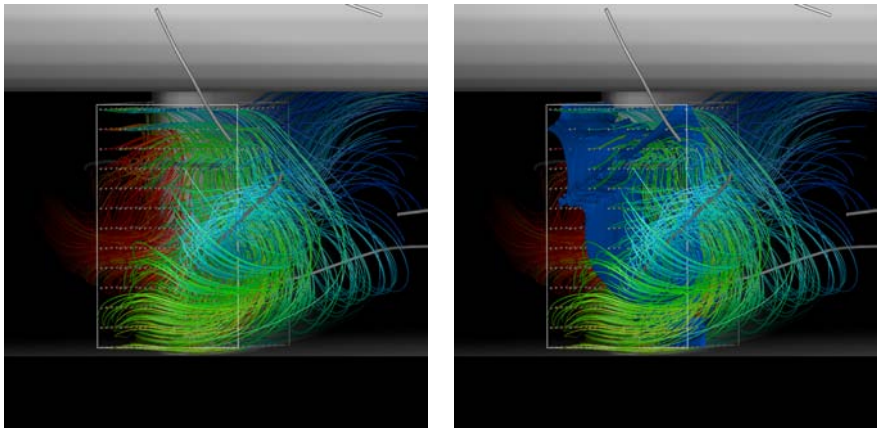

Fig. 2. Flow in Francis draft tube. Left: Vortex core lines (gray tubes) and some streamlines used for FTLE computation (arbitrary colored tubes started at white spheres). Right: Additionally instantaneous positive-time FTLE ridge visualizing the bifurcation at the divider.

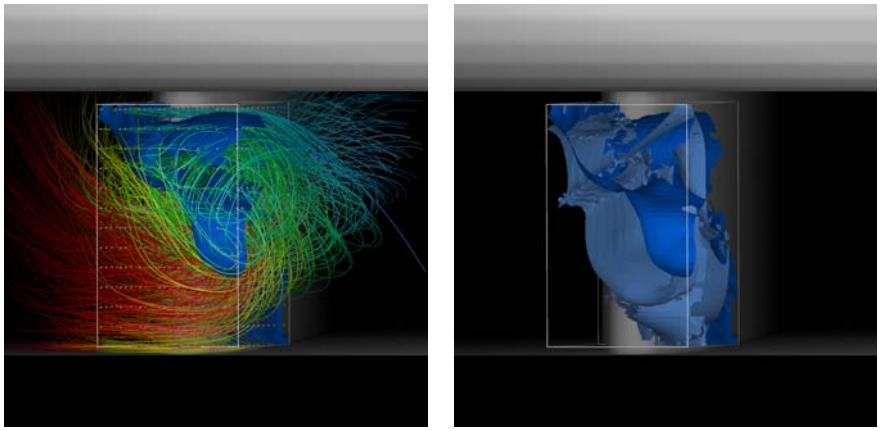

Fig. 3. Flow in Francis draft tube. Left: Unsteady positive-time FTLE ridge (blue) visualizing the bifurcation at the divider with some path lines used for FTLE computation (arbitrary colored tubes). Vortex core lines have been omitted because they move in time. Right: Comparing instantaneous positive-time FTLE ridge (light blue) with unsteady FTLE ridge.

than 5.5 were suppressed, as well as connected components smaller than 1000 triangles, and the computation took 774 seconds.

The second one is a vortex ring (vortex breakdown bubble) in the right channel of the draft tube. Figure 6 shows its unstable manifold and negative-time FTLE ridges. Interestingly, the corresponding ridge does not exhibit the bubble shape of the manifold, it is simply cylindrical, although consistent

To appear in: Topology-Based Methods in Mathematics + Visualization, Springer 2007

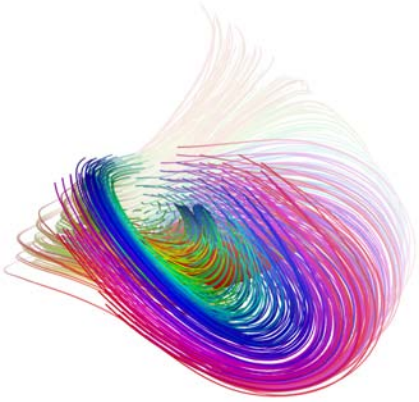

Fig. 4. Opposite view to the visualization of Figure 1 (left), with arbitrary-color tubes visualizing some of the positive-time streamlines.

Fig. 5. Steady positive-time FTLE ridges (blue) around vortex core line (gray tube) in front of the Francis divider.

with the fold of the manifold. FTLE was computed on a 60^3 grid with 4 seconds advection time, which took 704 seconds to compute. Ridge regions with $\lambda_n < 300$ were suppressed in order to remove noise, as well as connected components smaller than 2000 triangles.

3.5 Bifurcation in Pelton Distributor Ring

In this section, the steady CFD flow inside the distributor ring of a Pelton water turbine is examined using FTLE ridges. Figure 7 shows positive-time FTLE ridges computed at the sickle of the distributor ring. A sickle is a construct where part of the main flow is bifurcated into the injector that forms one of the jets that drive the turbine. One FTLE ridge shows clearly how the flow is split and an other FTLE ridge visualizes a recirculation zone. The FTLE was computed on a $100 \times 100 \times 40$ grid with advection time 0.1 seconds which took 1381 seconds. Ridge regions with FTLE smaller than 22 were suppressed as well as connected components smaller than 2000 triangles.

4 Conclusion

2D height ridges were extracted from 3D FTLE. Several ridge-filtering techniques were proposed in order to suppress noise but also for achieving physically significant visualizations. The ridges were compared to the results from vector field topology, usually resulting in a gain of information and interpretability.

To appear in: Topology-Based Methods in Mathematics + Visualization, Springer 2007

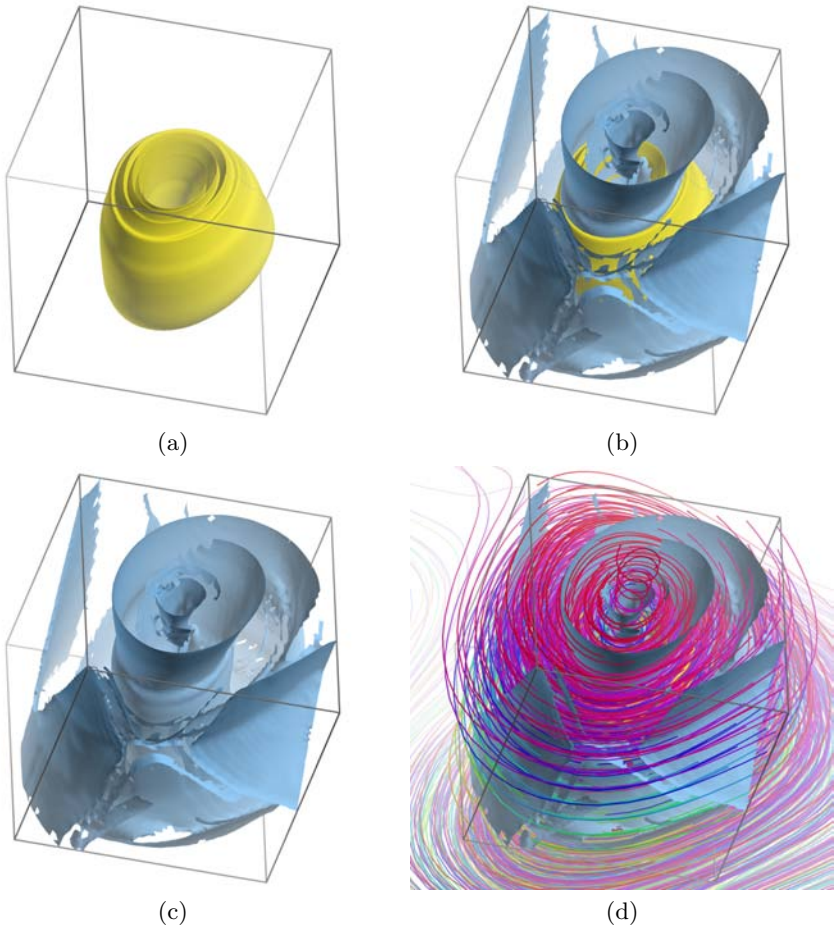

Fig. 6. Vortex breakdown bubble in Francis draft tube. (a) Unstable manifold of vortex breakdown bubble. (b) Same as (a) with instantaneous negative-time FTLE ridges. Ridge is consistent with fold. (c) Ridge from (b): cylindrical inside bubble. (d) Same as (b) with some negative-time streamlines used for FTLE computation.

References

[Asi93] Asimov, D.: Notes on the Topology of Vector Fields and Flows. Tech. Report RNR-93-003, NASA Ames Research Center (1993)

[Ebe96] David Eberly: Ridges in Image and Data Analysis. Computational Imaging and Vision. Kluwer Academic Publishers (1996)

[FP01] Furst, J.D., Pizer, S.M.: Marching Ridges. 2001 IASTED International Conference on Signal and Image Processing (2001)

[Hal01] George Haller: Distinguished material surfaces and coherent structures in three-dimensional fluid flows. Physica D 149 248–277 (2001)

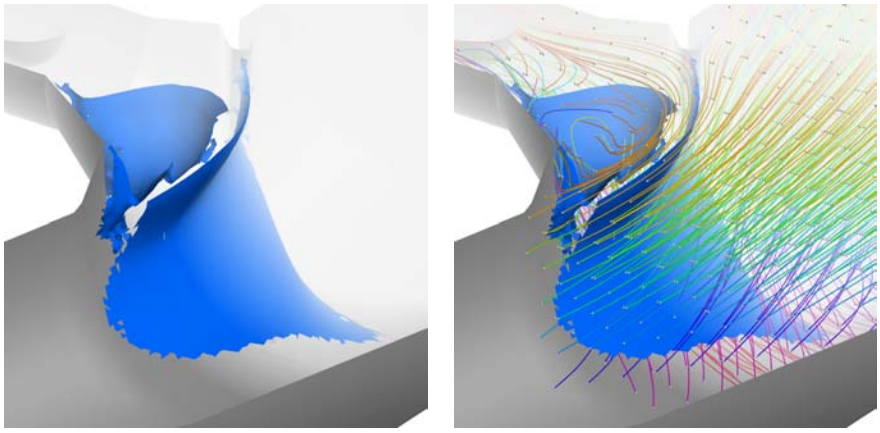

Fig. 7. Flow in Pelton distributor ring. Left: Positive-time FTLE ridges visualizing bifurcation at sickle and a recirculation region. Right: Additionally some positive-time streamlines used for FTLE computation, seeds are visualized by spheres.

[Hal02] George Haller: Lagrangian coherent structures from approximate velocity data. Phys. Fluids A14 1851–1861 (2002)

[Hal05] George Haller: An objective definition of a vortex. J. Fluid Mech. 525 1–26 (2005)

[HH89] James Helman, Lambertus Hesselink: Representation and Display of Vector Field Topology in Fluid Flow Data Sets. IEEE Computer **22**(8) 27–36 (1989)

[Hen66] Michel Henon: Sur la topologie des lignes de courant dans un cas particulier. Comptes Rendus Acad. Sci. Paris **262** 312–314 (1966)

[HZD98] De-Bin Huang, Xiao-Hua Zhao, Hui-Hui Dai: Invariant tori and chaotic streamlines in the ABC flow. Phys. Lett. A **237**(3) 136–140 (1998)

[KTW06] Gordon Kindlmann, Xavier Tricoche, Carl-Fredrik Westin: Anisotropy Creases Delineate White Matter Structure in Diffusion Tensor MRI. In: MICCAI'06, Lecture Notes in Computer Science 3749 (2006)

[LDS90] Yuval Levy, David Degani, Arnan Seginer: Graphical Visualization of Vortical Flows by Means of Helicity. AIAA **28**(8) 1347–1352 (1990)

[Lin96] Lindeberg, T.: Edge detection and ridge detection with automatic scale selection. International Journal of Computer Vision **30**(2) 77–116 (1996)

[Maj00] Peter Majer: A Statistical Approach to Feature Detection and Scale Selection in Images. Ph.D. thesis, University of Goettingen (2000)

[STW*06] Kuangyu Shi, Holger Theisel, Tino Weinkauf, Helwig Hauser, Hans-Christian Hege, Hans-Peter Seidel: Path Line Oriented Topology for Periodic 2D Time-Dependent Vector Fields. Proc. Eurographics / IEEE VGTC Symposium on Visualization (EuroVis '06) 139–146 (2006)

[TWH*03] Holger Theisel, Tino Weinkauf, Hans-Christian Hege, Hans-Peter Seidel: Saddle Connectors - An Approach to Visualizing the Topological Skeleton of Complex 3D Vector Fields. Proc. IEEE Visualization 225–232 (2003)

[TWH*04] Holger Theisel, Tino Weinkauf, Hans-Christian Hege, Hans-Peter Seidel: Stream Line and Path Line Oriented Topology for 2D Time-Dependent Vector Fields. Proc. IEEE Visualization 321–328 (2004)

To appear in: Topology-Based Methods in Mathematics + Visualization, Springer 2007

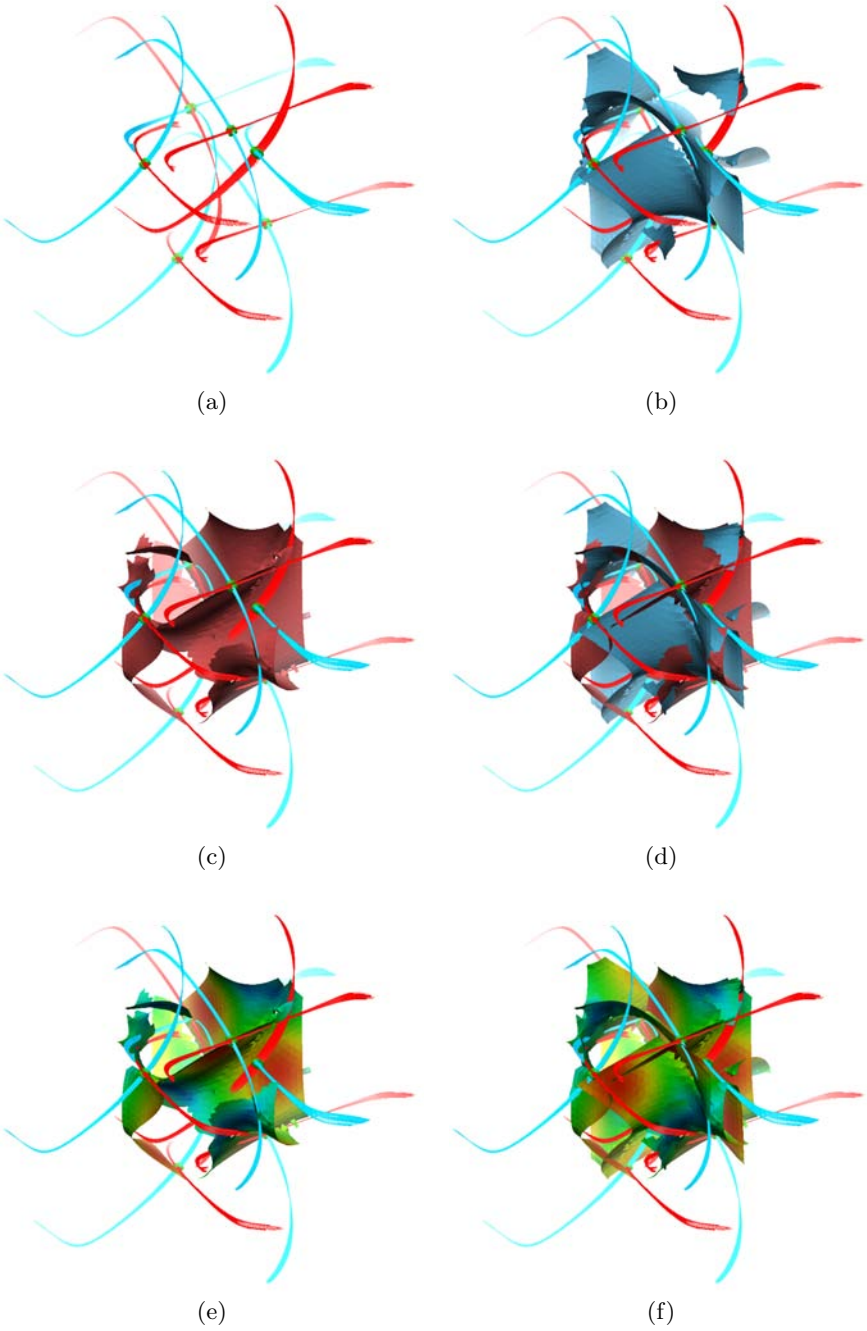

Fig. 8. ABC flow. (a) Seeds around critical points (green spheres), and corresponding streamlines in positive time (red) and negative time (blue). 2D manifolds are 1D-degenerate. (b) Same as (a) with additional positive-time FTLE ridges. (c) Same as (b) but with negative-time FTLE ridges instead of positive-time FTLE ridges (red). (d) Positive-time FTLE ridges (blue) and negative-time FTLE ridges (red). Ridges are well consistent with manifolds. (e) Same as (a) with negative-time FTLE ridges colored with short negative-time FTLE. (f) Additionally positive-time FTLE ridges colored with short positive-time FTLE.

To appear in: Topology-Based Methods in Mathematics + Visualization, Springer 2007

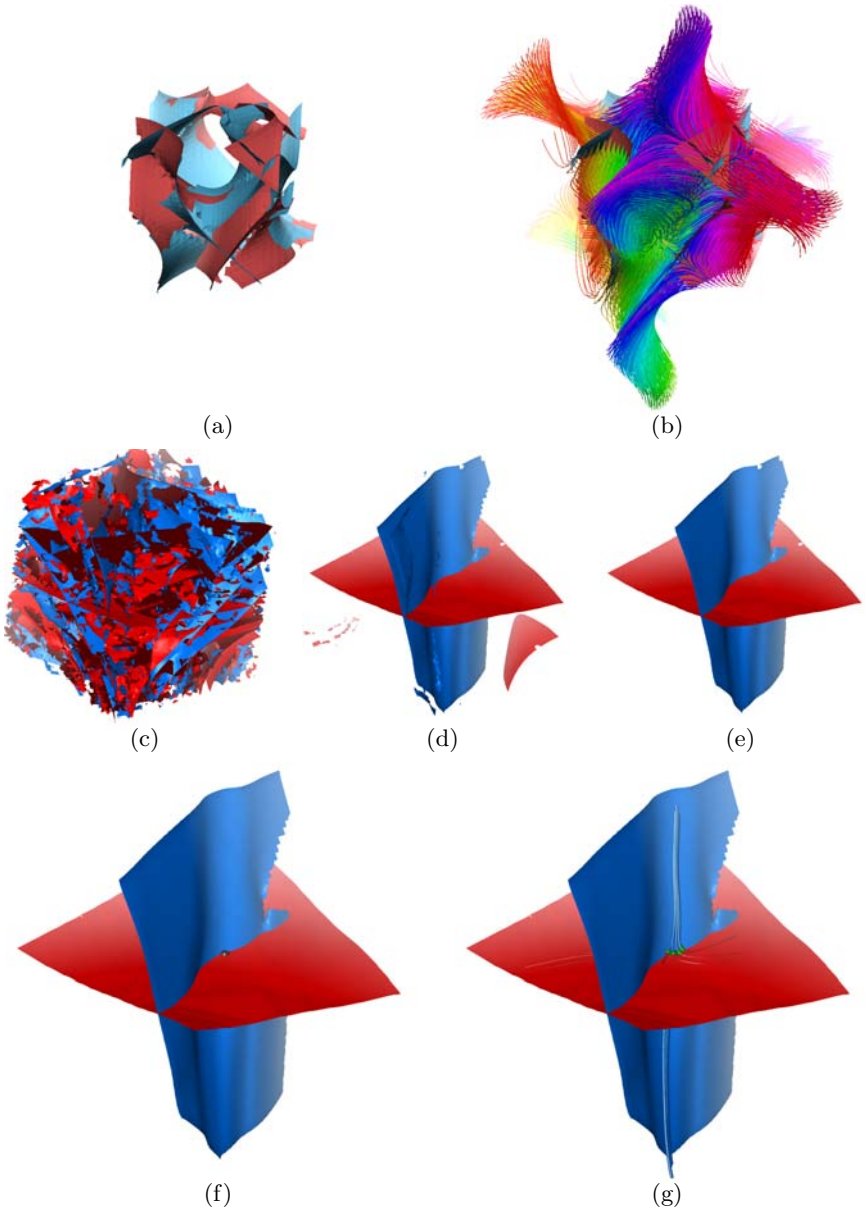

Fig. 9. (a)–(b): another view to the FTLE ridges from Figure 8(d) of the ABC flow. (c)–(g): 3D saddle in Francis draft tube. Positive-time FTLE ridges (blue) and negative-time FTLE ridges (red). (a) FTLE ridges. (b) Additionally positive-time trajectories (arbitrary colors) started from nodes inside the first period of the ABC flow, as used for FTLE computation. Trajectories are well consistent with FTLE ridges. (c) No filtering. (d) Minimum FTLE 3.5 (positive-time) and 4.0 (negative-time). (e) Additionally to (e) suppressing components smaller than 1000 (positive-time) and 4000 triangles (negative-time). (f) Critical point (black) is close to the intersection curve of the two ridges. (g) Seeds around critical point (green) and streamlines in positive time (red) and negative time (blue) from seeds. Streamlines visualizing the 1D manifold of the saddle lie inside positive-time FTLE ridge.